Biallelic Mutations in *MITF* Cause Coloboma, Osteopetrosis, Microphthalmia, Macrocephaly, Albinism, and Deafness

Aman George,[1] Dina J. Zand,[2,6] Robert B. Hufnagel,[1] Ruchi Sharma,[3] Yuri V. Sergeev,[1] Janet M. Legare,[4] Gregory M. Rice,[4] Jessica A. Scott Schwoerer,[5] Mariana Rius,[1,7] Laura Tetri,[4] David M. Gamm,[4,5] Kapil Bharti,[3,8] and Brian P. Brooks[1,2,8,*]

Human *MITF* is, by convention, called the "microphthalmia-associated transcription factor" because of previously published seminal mouse genetic studies; however, mutations in *MITF* have never been associated with microphthalmia in humans. Here, we describe a syndrome that we term COMMAD, characterized by coloboma, osteopetrosis, microphthalmia, macrocephaly, albinism, and deafness. COMMAD is associated with biallelic *MITF* mutant alleles and hence suggests a role for *MITF* in regulating processes such as optic-fissure closure and bone development or homeostasis, which go beyond what is usually seen in individuals carrying monoallelic *MITF* mutations.

Mouse *Mitf* encodes a basic helix-loop-helix zipper protein critical for the development of neural-crest-derived melanocytes, neuroectoderm-derived retinal pigment epithelium (RPE) cells, and hematopoietic-tissue-derived osteoclasts and mast cells. Autosomal-dominant *MITF* mutations are associated with two highly overlapping deafness and pigmentation disorders: Waardenburg syndrome type 2A (WS2A [MIM: 193510])[1] and Tietz syndrome (MIM: 103500).[2] Congenital pigmentation defects and sensorineural deafness are attributed to the role of *MITF* in differentiation and survival of melanocytes in skin and stria vascularis of the cochlea, respectively.[3] Autosomal-recessive or compound-heterozygous inheritance of *MITF* has not been reported previously in humans. Here, we describe two unrelated individuals with compound-heterozygous *MITF* mutations resulting in a complex phenotype that we term COMMAD (coloboma, osteopetrosis, microphthalmia, macrocephaly, albinism, and deafness) and investigate the underlying molecular mechanisms. Biochemical and functional data for one of the probands demonstrate that mutations do not affect dimerization of MITF with other MiT family transcription factors but rather alter nuclear migration and DNA binding of homo- and heterodimers and thus allow the mutant alleles to act as dominant negative. These observations are in agreement with those of previous studies on the $Mitf^{mi/mi}$ mouse model, where homozygosity of the dominant-negative *mi* allele causes a similar phenotype.[4,5]

At last examination, proband I was a 5-year, 3-month-old male with colobomatous microphthalmia and microcornea with pannus, dense bilateral cataracts, translucent irides, profound congenital sensorineural hearing loss, and a lack of visible pigment in the hair, skin, and eyes (Figures 1A–1C). Microphthalmia was first detected on prenatal ultrasound. Head circumference was 56.0 cm (>3 SDs for age), consistent with macrocephaly, and weight (17.3 kg [−0.5 SD]) and height (110.0 cm [0.0 SD]) were normal for his age. He had facial dysmorphisms including frontal bossing, shallow orbits, preauricular pits, and posteriorly rotated ears. Skeletal features included a prominent frontal bone, diffuse expansion of the anterior ends of the ribs (Figure 1D, arrow), and bilateral fifth-finger clinodactyly (data not shown). A radiographic skeletal survey performed at 13 months of age showed osteopetrosis (Figure 1D, arrowheads depict areas of increased bone density). Axial magnetic resonance imaging (MRI) of the brain showed small eyes (~7–8 mm, line on Figure 1E), optic nerves, and chiasm with mild prominence of ventricles, but no other structural abnormalities (Figure 1E). He was delivered at term after an uneventful pregnancy to nonconsanguineous parents, both of whom have congenital sensorineural hearing loss, blue irides, fair skin, and premature graying of the hair and are in their third or fourth decade. One male sibling was affected similarly to his parents, and one sister was unaffected (Figure 1F).

At last exam, proband II was a 9-month-old female born with severe microphthalmia, profound congenital sensorineural hearing loss, and a lack of pigment in the hair, skin, and eyes (Figures 1G–1I). She had relative macrocephaly (43.0 cm [0 SD for age]), short stature (65.0 cm [−2 SDs]),

[1]Ophthalmic Genetics and Visual Function Branch, National Eye Institute, NIH, Bethesda, MD 20892, USA; [2]Children's National Medical Center, Washington, DC 20010, USA; [3]Unit on Ocular and Stem Cell Translational Research, National Eye Institute, NIH, Bethesda, MD 20892, USA; [4]Department of Pediatrics, University of Wisconsin School of Medicine and Public Health, Madison, WI 53726, USA; [5]McPherson Eye Research Institute and Department of Ophthalmology and Visual Sciences, University of Wisconsin School of Medicine and Public Health, Madison, WI 53726, USA
[6]Present address: Office of New Drugs, Office of Drug Evaluation III Division of Gastroenterology and Inborn Errors Products, US Food and Drug Administration, Silver Spring, MD 20993, USA
[7]Present address: School of Marine and Atmospheric Sciences, Stony Brook University, Stony Brook, NY 11790, USA
[8]These authors contributed equally to this work
*Correspondence: brian.brooks1@nih.gov
http://dx.doi.org/10.1016/j.ajhg.2016.11.004.

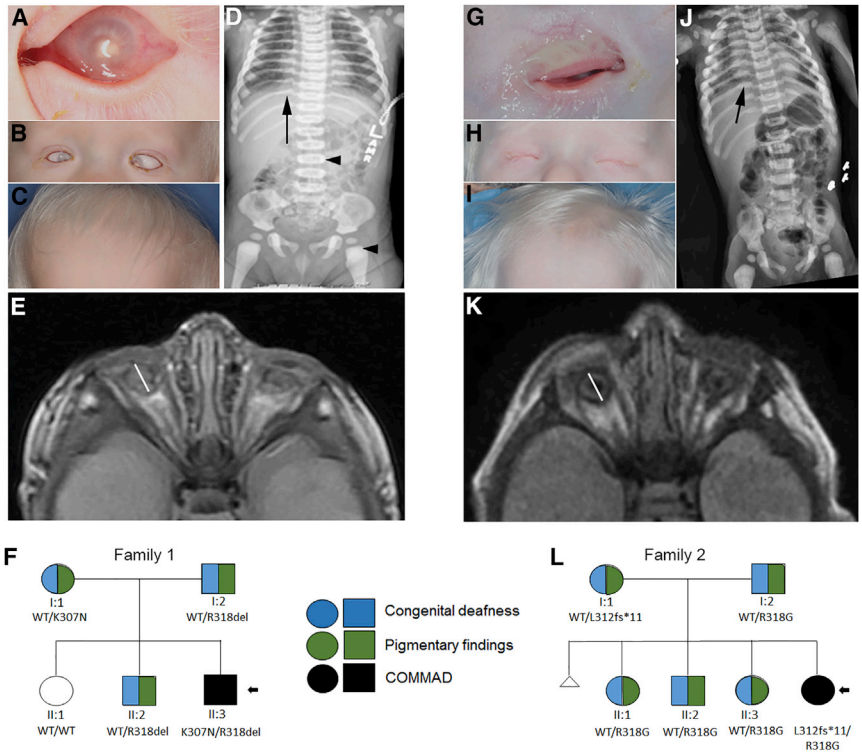

Figure 1. Clinical Features of COMMAD Syndrome

(A–K) COMMAD-affected probands I (A–E) and II (G–K) had microphthalmia and shallow orbits (A and G) with frontal bossing (B and H) and platinum hair (C and I). Additionally, osteopetrosis was noted, prominently in the anterior ribs (arrows) and femoral head (arrowheads) (D and J). Microphthalmia (8 mm line across optic globe) with associated optic-nerve and chiasm hypoplasia was confirmed on brain MRI (E and K), but other structures were normal.

(F and L) Pedigrees of family 1 (F) and family 2 (L).

and low weight (5.2 kg [<−3 SDs]). She had skeletal findings (Figure 1J) and craniofacial dysmorphisms similar to those of proband I, with the addition of micrognathia and wide palatine ridges. She had mild hypotonia throughout. Brain MRI revealed severe microphthalmia (globes 8 mm bilaterally, line on Figure 1K) and small optic nerves, as well as a cavum septum pellucidum et vergae variant and otherwise normal brain structures (Figure 1K). She was also born to non-consanguineous parents, both of whom have congenital sensorineural hearing loss, premature graying, blue irides, and fair skin. She has one male and two female siblings affected similarly to her parents (Figure 1L). Renal ultrasound was normal for both probands.

Interestingly, the phenotypes of probands I and II share homology with the phenotype of mice homozygous for the *Mitf mi* allele ($Mitf^{mi/mi}$)[4,5] and are unlike that of any previously reported individuals with heterozygous *MITF* mutations.[6,7] Clinical diagnosis of Waardenburg syndrome type 2 in the parents and affected siblings prompted sequencing of *MITF*. Both families were previously unreported. DNA samples were collected after approval by the NIH institutional review board (protocol 06-EI-0169). Informed consent or assent for DNA storage, mutation analysis, and publication of images was obtained from all subjects. Sanger sequencing of the entire *MITF* coding sequence, including intron-exon boundaries, performed in a laboratory certified by the Clinical Laboratory Improvement Amendments, revealed two mutations in proband I: paternally inherited *MITF* mutation c.952_954delAGA (p.Arg318del in the isoform MITF-A [GenBank: NM_198159.2], corresponding to p.Arg217del in the isoform MITF-M [GenBank: NM_000248.1]), known to cause WS2A and Tietz syndrome;[8] and a maternally inherited, previously unreported *MITF* mutation, c.921G>C (p.Lys307Asn in the isoform MITF-A). This latter mutation is not reported in 1000 Genomes, dbSNP, NHLBI Exome Sequencing Project (ESP) Exome Variant Server, or the Exome Aggregation Consortium (ExAC) Browser and was predicted to be deleterious with a CADD score of 26. Alteration of Lys307 to Gln, another polar amine-group amino acid, is associated with WS2A.[9] A male sibling diagnosed with WS2A was heterozygous for the paternal allele (Figure 1F). The unaffected sister had neither mutation. Proband II was also observed to be compound heterozygous for the paternally inherited c.952A>G (p.Arg318Gly) missense mutation and maternally inherited c.938−1G>A, a canonical splice-site mutation resulting in a truncated protein (p.Leu312fs*11). None of the affected individuals from both families displayed dystopia canthorum, consistent with a WS2A diagnosis, and none had osteopetrosis, macrocephaly, microphthalmia, or colobomata.

Heteroallelic combinations in *Mitf* mutant mice have been studied extensively, and only compound heterozygosity of dominant-negative alleles causes the most severe COMMAD-like phenotype. Because MITF p.Arg318del is a known dominant-negative variant, we next studied the functional impact of the c.921G>C (p.Lys307Asn) *MITF* mutation observed in proband I and his mother. The open reading frame of human *MITF* (catalog no. FXC03436, Promega; GenBank: NM_198159) was obtained, and isoforms MITF-A and MITF-D were amplified from it (for primer and probe sequences, see Table S1). All experiments were performed in the context of MITF-A (1,563 bp; GenBank: NP_937802.1), the most widely expressed isoform, as opposed to MITF-M (GenBank: NP_000239.1), on which most of the previous studies were based.[10,11] Experiments were repeated with MITF-D (1,407 bp), an isoform expressed only in RPE. For detailed methodology, refer to the Supplemental Data.

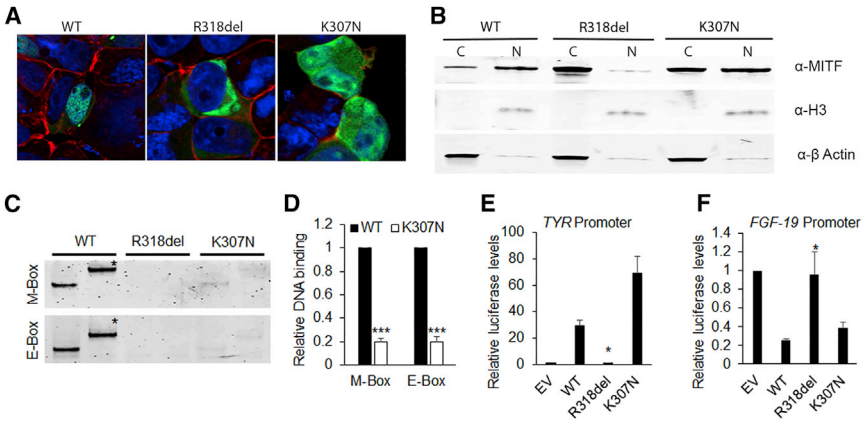

Figure 2. Nuclear Migration, DNA Binding, and Promoter Regulatory Potential of WT and Mutant MITF-A Isoforms

HEK293 cells were cultured in DMEM with 10% FBS and 1% penicillin-streptomycin for 24 hr and then transiently transfected with fluorescent-protein-tagged wild-type (WT) or mutant MITF constructs with X-tremeGENE HP (Roche) according to the manufacturer's instructions. Cells were fixed with 4% paraformaldehyde 24 hr after transfection, stained with Phalloidin (red) and DAPI, and photographed at 60× magnification with a confocal microscope. (A) GFP-tagged WT MITF-A isoform was observed predominantly in the nucleus of cells. The p.Arg318del mutant was observed only in the cytoplasm, whereas p.Lys307Asn localized in both the cytoplasm and nucleus, suggesting some disruption of the nuclear migration ability (also see Movie S1).

(B) Subcellular localization of the mutants was further confirmed by western blot analysis of the cytoplasmic (C) and nuclear (N) fractions of cells transfected by WT and mutant MITF-A, in agreement with the fluorescence microscopy data. For protein blotting, cytoplasmic and nuclear fractions were separated with the Nuclear Extract Kit (Active Motif) according to the manufacturer's instructions. 20 μg of protein (BCA Protein Assay Kit, Life Technologies) was separated by SDS-PAGE on polyacrylamide gels (Bio-Rad). Proteins were transferred onto polyvinylidene fluoride membranes (Bio-Rad) and probed with mouse monoclonal antibody to MITF (clone D5, Thermo Scientific). Rabbit polyclonal antibody to histone H3 and β-actin (Abcam) were used as loading controls. Membranes were then incubated with secondary antibodies (1:10,000; LI-COR) and then scanned with the Odyssey infrared scanner and analyzed with Image Studio Lite v.4.0 (LI-COR).

(C) Electrophoretic mobility shift assay (EMSA) was performed with DNA oligonucleotides harboring M-box and E-box consensus sequences (Table S2) labeled with IR700 dye (Integrated DNA Technologies) with the Odyssey Infrared EMSA Kit (LI-COR) as per the manufacturer's instructions. WT and mutant MITF isoforms were in vitro translated with the SP6 TnT Quick Coupled Transcription/Translation System (Promega) as per the manufacturer's instructions. 50 femtoM of duplex oligonucleotide was mixed with binding buffer (100 cmM Tris, 500 mM KCl, and 10 cmM DTT [pH 7.5]), poly(deoxyinosinic-deoxycytidylic), 1 M KCl, and the WT and/or mutant protein in vitro translation mix, incubated for 30 min at room temperature, and then separated on 5% TBE polyacrylamide gels (Bio-Rad) at 100V. The gels were scanned with an Odyssey scanner and analyzed with Image Studio Lite v.4.0 (LI-COR). M-box and E-box sequences showed strong DNA binding by WT MITF-A, no DNA binding by the p.Arg318del mutant, and significantly reduced binding by the p.Lys307Asn mutant. A supershift (*), produced by MITF-specific antibody, confirmed the specificity of MITF and DNA binding (also see Figure S2).

(D) Quantification of the DNA binding by WT and p.Lys307Asn MITF-A, as calculated from three different trials.

(E and F) The Dual-Luciferase Reporter Assay System (Promega) was used to study the promoter regulatory potential of WT and mutant MITF-A isoforms. With X-tremeGENE HP (Roche), HEK239T cells (1×10^5 seeding density) were co-transfected 24 hr after seeding with 100 ng of MITF-A or -D isoforms, 200 ng of luciferase-promoter reporter construct, 1:1,000 *Renilla* luciferase vector (pRL Null Renilla), and empty vector to equalize the amount of transfected DNA. All transfections were performed in duplicate. Transfected cells were lysed 24 hr after transfection, and aliquots were used for determining firefly and *Renilla* luciferase activities in triplicate. Data were normalized to the activity of *Renilla* luciferase. All experiments were repeated three times. The WT and p.Lys307Asn mutant MITF-A activated the *TYR* promoter and repressed the *FGF19* promoter. The p.Arg318del mutant showed no promoter regulatory potential. All comparisons are in reference to the WT MITF; error bars represent standard errors p values were calculated with the two-sided Student's t test: *$p < 0.05$, **$p < 0.01$, ***$p < 0.005$.

In our study, GFP-tagged wild-type (WT) MITF demonstrated predominantly nuclear localization (Figures 2A and 2B; Figure S1) and strong M-box (TCATGTG) and E-box (CACGTG) binding (Figures 2C and 2D; Figure S2). GFP-tagged MITF-A p.Arg318del mutant isoforms (Figures 2A and 2B; Figure S1) did not migrate to the nucleus in transfected HEK293 cells or bind consensus M-box or E-box DNA sequences in vitro (Figures 2C and 2D; Figure S2). This is most likely due to the fact that the positively charged arginine residue is a part of nuclear-localizing signal (ERRRRF) and is directly involved in interactions with the negatively charged DNA phosphate backbone (Figures S3A–S3C). This allele neither activated the tyrosinase (*TYR* [MIM: 606933]) promoter nor repressed the *FGF19* (MIM: 603891) promoter in dual luciferase reporter assays (Figures 2E and 2F; Figures S4A and S4B). Previously, WS2A-associated p.Arg318del and p.Arg318Gly proteins were demonstrated to lack DNA binding or regulate target-gene promoters, despite reported nuclear localization of the corresponding human MITF-M.[12] In comparison, the MITF-A p.Lys307Asn mutant distributed equally between the nucleus and the cytoplasm (Figures 2A and 2B; Figure S1), indicating a partial requirement for the charged p.Lys307 residue for nuclear translocation of the human MITF-A and MITF-D isoforms. Furthermore, compared with WT MITF, p.Lys307Asn MITF-A or MITF-D had only ~20% DNA-binding ability in vitro, correlating with the loss of a positively charged amino acid (Figures 2C and 2D; Figures S2E and S2F). The p.Lys307Asn protein, nevertheless, had significant transcriptional regulatory potential on *TYR* and *FGF19* promoters (Figures 2E and 2F; Figures S4A and S4B).

The mouse *Mitf mi* allele (similar to p.Arg318del of proband I) acts in a dominant-negative manner on MiT family

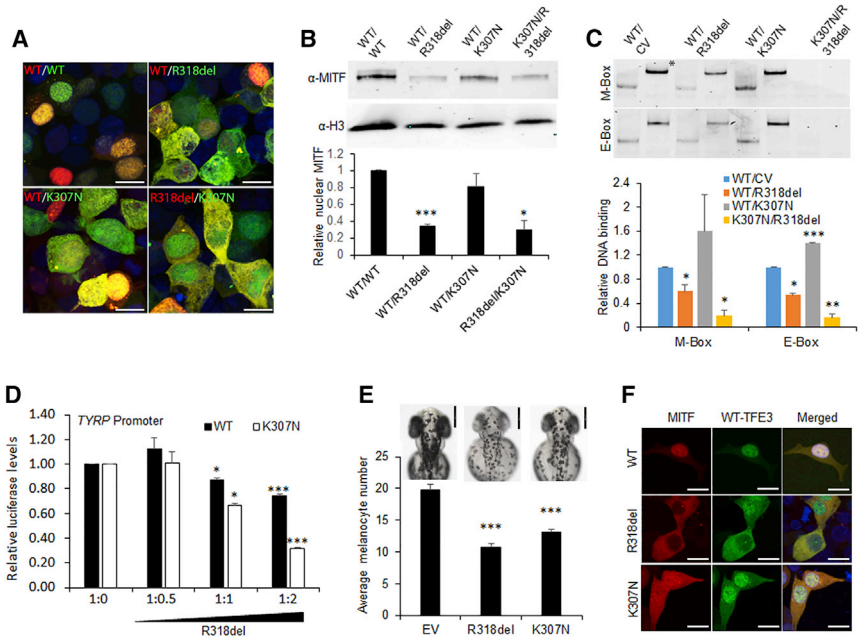

Figure 3. The Nuclear Migration, DNA Binding, and Promoter Regulatory Potential of WT MITF in the Presence of Mutant MITF Isoforms

(A) Nuclear-cytoplasmic distribution of MITF in the presence of the mutants (scale bars represent 10 μm) was studied by confocal microscopy. The WT and mutant MITF were differentially tagged by GFP or RFP.

(B) Amounts of nuclear MITF were calculated by western blotting from three different experiments and are represented as a graph.

(C) EMSA gels representative of three experiments show DNA-binding ability of the WT-control-vector (CV), WT-p.Arg318del, WT-p.Lys307Asn, and p.Arg318del-p.Lys307Asn combinations (*supershifted band) to the M-box and E-box DNA sequences.

(D) The dominant effect of p.Arg318del on WT and p.Lys307Asn proteins was studied by a dual luciferase reporter assay with the *TYRP* promoter. In increasing concentrations (0, 50, 100, and 200 ng), p.Arg318del was co-transfected with a constant amount of WT or p.Lys307Asn (100 ng), along with 200 ng of a luciferase-promoter construct (*TYRP* or *FGF19*), 1:1,000 *Renilla* luciferase vector, and empty vector to equalize the amounts of transfected DNA. The p.Arg318del mutant in increasing amounts had a dominant-negative effect on WT MITF (solid bars) and p.Lys307Asn (open bars).

(E) Effect of mutant zebrafish *mitfa* overexpression on the average melanocyte numbers of 36 hpf zebrafish embryos. The WT ABTL strain of zebrafish was maintained under standard conditions of fish husbandry according to NIH Animal Use and Care Committee guidelines. WT *mitfa* and the isoforms harboring the two human mutations, cloned in pCS2+, were linearized and injected into the cells of freshly fertilized zebrafish eggs at the single-cell stage. Linearized pCS2+ vector (EV) was also injected in equal amounts as an experimental control. The volume of injection solution per embryo was ~1 nL. The melanocytes on a specified dorsal-trunk region of 34–36 hpf zebrafish embryos were photographed and then counted for 30 different embryos pooled from three different trials. Representative images of 48 hpf embryos are shown (scale bars represent 0.1 mm).

(F) Nuclear localization of TFE3 in the presence of the two MITF mutants (scale bars represent 10 μm) was studied by confocal microscopy. All comparisons are in reference to the WT MITF or EV; error bars represent standard error p values were calculated with the two-sided Student's t test: *$p < 0.05$, **$p < 0.01$, ***$p < 0.005$.

transcription factors by dimerizing with them and interfering with their nuclear localization.[11] Dominant-negative mutations in *MITF* typically affect either the DNA-binding domain or the transcriptional-activation domain, leaving the dimerization domains unaffected.[10] Consistent with this observation, homozygosity of the *Mitf or* (oak ridge) allele (ERR[R/K]RF, proximal to ERRR[R/G]F of proband II) or *Mitf wh* allele (Ile212Asn) in mice results in some of the salient features of COMMAD, such as a white coat, osteopetrosis, and ocular malformations including microphthalmia and anophthalmia.[5] To account for the clinical phenotype of the probands, we studied the interactions between p.Arg318del and p.Lys307Asn proteins, as well as their interaction with WT MITF. Our results showed that co-expression of p.Arg318del and p.Lys307Asn proteins in HEK293 cells resulted in migration of only 30% of MITF into the nucleus, whereas co-expression of the p.Arg318del or p.Lys307Asn mutant and the WT protein resulted in 36% or 81% migration, respectively (Figures 3A and 3B and Movie S1). Electrophoretic mobility shift assay (EMSA) showed that DNA binding of co-in-vitro-translated mutant proteins (p.Arg318del and p.Lys307Asn in equal amounts) was <20% of that of WT MITF for consensus E-box and M-box elements. A WT-p.Arg318del combination resulted in ~50% reduction of DNA binding, whereas WT-p.Lys307Asn bound both consensus elements better than a WT-control-vector combination (Figure 3C). These results were further supported by in silico DNA-binding simulations (Figure S3D). Furthermore, transcriptional activation of the *TYRP1* (MIM: 115501) promoter was reduced more dramatically when p.Lys307Asn was co-expressed with increasing amounts of p.Arg318del (Figure 3D, open bars) than when the WT protein was co-expressed with increasing amounts of p.Arg318del (Figure 3D, solid bars). Transcriptional repression of the *FGF19* promoter by MITF was similarly impaired when p.Lys307Asn was co-expressed with increasing amounts of p.Arg318del (Figure S4C, open bars). The subcellular-localization data together with DNA-binding and promoter regulatory studies suggest that the p.Arg318del-p.Lys307Asn combination would significantly diminish MITF activity more than either variant present in combination with the WT protein.

Heterozygous *MITF* mutations in humans cause sensorineural deafness and pigmentation defects distinct from complete albinism. Fully penetrant albinism in the

individuals with COMMAD syndrome suggests that MITF function is below the critical threshold required for melanocyte migration, differentiation, and survival. To investigate the effects of these mutants on pigmentation in vivo, we introduced the two analogous human mutations into zebrafish *mitfa* cDNA (homologous to human MITF-M) and injected them as expression constructs into 1-cell-stage zebrafish embryos. Melanocytes in a specified dorsal-trunk region were quantified at 34–36 hr post-fertilization (hpf). As expected, injection of p.Arg318del mutant MITF resulted in a significantly lower number of melanocytes than did injection of similar amounts of empty vectors. Injection of p.Lys307Asn also led to significantly reduced melanocyte numbers (Figure 3E), consistent with its effects observed in vitro.

Mitf$^{mi/mi}$ mice exhibit colobomatous microphthalmia, which has never been reported for human *MITF* mutations. The severe eye phenotype observed in COMMAD syndrome could be attributed to the deregulation of genes involved in the development of RPE and the neural retina.[13,14] For instance, FGF15 in mice (homologous to human FGF19) is a direct target of MITF and plays an important role in retinal differentiation. We therefore performed a reporter assay by using the RPE-specific *Best1* promoter[15] and observed that the p.Arg318del-p.Lys307Asn combination showed significantly less transactivation of the *Best1* promoter than the WT-WT, WT-p.Arg318del, and WT-p.Lys307Asn combinations (Figure S4D). These data fit well with the observation that only biallelic *MITF* mutations in mice and humans result in severe eye phenotypes. Our study provides evidence that *MITF* mutations can cause colobomatous microphthalmia in humans.

MITF acts as a heterodimer with Mi-T family transcription factors TFE3, TFEB, and TFEC.[10] Osteopetrosis in *Mitf* mutant mice has been observed only with homozygosity of semi-dominant mutant alleles, e.g., in *Mitf*$^{mi/mi}$ mice. In these mice, MITF interferes with the activity of binding partner TFE3, which is important for osteoclast function. Consistent with this, osteoclasts are normal in *Mitf*- or *Tfe3*-null mice, whereas combined loss of both proteins results in severe osteopetrosis.[16] In HEK293 cells, we observed cytoplasmic retention of GFP-tagged TFE3 when it was co-expressed with RFP-tagged p.Arg318del or p.Lys307Asn, but not when it was co-expressed with WT MITF (Figure 3F). In contrast to COMMAD syndrome, none of the reported cases of human *MITF* mutations exhibit osteopetrosis, suggesting that the two mutant alleles together exert a stronger dominant-negative effect on the entire Mi-T family than a single dominant-negative allele.

Developmentally, mouse *Mitf* expression is tightly regulated and is first detected throughout the optic vesicle of 22-somite-stage embryos, followed by expression in presumptive RPE of the optic cup.[17] Shortly after its detection in the eye, *MITF* expression is also observed in neural-crest-derived melanoblasts, which are melanocyte precursors.[18] Quite interestingly, early eye development is normal in individuals with heterozygous *MITF* mutations, but the spectrum of pigmentation and sensorineural defects varies greatly.[19] Also, retinal-pigmentation defects in humans are observed only with the dominant-negative allele.[19] In adult mice, *Mitf* expression is observed in osteoclasts,[20] mast cells,[21] heart, and skeletal muscle,[22] in addition to melanocytes and RPE. The *Mitf*$^{mi/mi}$ mouse displays defects in all of these cell and tissue types. Although heterozygous human *MITF* mutations in Waardenburg and Tietz syndromes are not associated with these defects, apart from pigmentation and related sensorineural defects,[8] all of the COMMAD syndrome phenotypes associate well with abnormalities observed in the *Mitf*$^{mi/mi}$ mouse.

To our knowledge, no published reports have shown a complete phenotypic overlap with the clinical features of COMMAD syndrome. Mutations in *MAF* (associated with Ayme-Gripp syndrome [MIM: 601088]) cause coloboma, congenital cataracts, sensorineural deafness, intellectual disability, and dysmorphic facies, among others.[23] Some other genes known to cause syndromic or non-syndromic uveal coloboma—such as *PAX6* (MIM: 607108), *SHH* (MIM: 600725), *GDF3* (MIM: 606522), *RBP* (MIM: 180250), *CHX10* (MIM: 142993), *SOX2* (MIM: 184429), *OTX2* (MIM: 600037), and *RAX* (MIM: 601881)—result in a range of ocular phenotypes, including microphthalmia, cataracts, and microcornea. None of the reported incidences of syndromic or isolated cases of coloboma have been associated with albinism or osteopetrosis. Moreover, these abnormalities have not been reported previously for human *MITF* disorders. Description of this syndrome is perhaps particularly important, given that intermarriage within the deaf community is relatively common, and neither set of parents in this study recognized they had WS2A prior to having their child with COMMAD. We would also stress the need for genotyping individuals suspected to have Waardenburg syndrome at the molecular level and providing appropriate genetic counselling.

In summary, we report an *MITF* allele (c.921G>C [p.Lys307Asn]) that causes WS2A and, when present with the dominant-negative allele (c.952_954delAGA [p.Arg318del]), results in a syndrome that we have termed COMMAD. This condition was seen again in another person with a probably dominant-negative mutation (p.Arg318Gly) and a canonical splice-site mutation (c.938−1G>A). We propose that an allelic combination involving at least one dominant-negative mutation, inherited in a recessive manner, represents the underlying molecular mechanism leading to COMMAD syndrome, thus delineating important roles for *MITF* in ocular morphogenesis and bone homeostasis in humans.

Supplemental Data

Supplemental Data include four figures, one table, and one movie and can be found with this article online at http://dx.doi.org/10.1016/j.ajhg.2016.11.004.

Acknowledgments

We are grateful to the probands and their families. We thank Dr. Heinz Arnheiter for critical comments on the manuscript, Dr. James Lister (Virginia Commonwealth University, Richmond, VA) for the zebrafish *mitfa* construct, Drs. Noriko Esumi (Wilmer Eye Institute, Johns Hopkins University, Baltimore, MD) and Sridhar Mani (Albert Einstein College of Medicine, Bronx, NY) for luciferase promoter constructs, Drs. Chun Gao and Robert Farris (Biological Imaging Core, National Eye Institute [NEI]) for expert assistance with confocal laser-scanning microscopy experiments, Ramakrishna Alur for technical assistance, Delphine Blain for genetic counseling, the NEI Clinical Photography Section for outstanding technical assistance, and Anna Larson and Tyler Fayard for zebrafish breeding and maintenance. This work was supported by the intramural program of the NEI.

Received: May 12, 2016
Accepted: October 25, 2016
Published: November 23, 2016

Web Resources

1000 Genomes, http://www.1000genomes.org/
Combined Annotation Dependent Depletion (CADD), http://cadd.gs.washington.edu/
dbSNP, http://www.ncbi.nlm.nih.gov/SNP/
Exome Aggregation Consortium (ExAC) Browser, http://exac.broadinstitute.org/
NHLBI Exome Sequencing Project (ESP) Exome Variant Server, http://evs.gs.washington.edu/
OMIM, http://www.omim.org/
RCSB Protein Data Bank, http://www.rcsb.org/pdb/home/home.do
RefSeq, https://www.ncbi.nlm.nih.gov/refseq/
UCSF Chimera, http://www.cgl.ucsf.edu/chimera/
UniProt: MITF, http://www.uniprot.org/uniprot/O75030
YASARA, http://www.yasara.org/

References

1. Waardenburg, P.J. (1951). A new syndrome combining developmental anomalies of the eyelids, eyebrows and nose root with pigmentary defects of the iris and head hair and with congenital deafness. Am. J. Hum. Genet. *3*, 195–253.
2. Tietz, W. (1963). A syndrome of deaf-mutism associated with albinism showing dominant autosomal inheritance. Am. J. Hum. Genet. *15*, 259–264.
3. Price, E.R., and Fisher, D.E. (2001). Sensorineural deafness and pigmentation genes: melanocytes and the Mitf transcriptional network. Neuron *30*, 15–18.
4. Hero, I. (1989). The optic fissure in the normal and microphthalmic mouse. Exp. Eye Res. *49*, 229–239.
5. Steingrímsson, E., Moore, K.J., Lamoreux, M.L., Ferré-D'Amaré, A.R., Burley, S.K., Zimring, D.C., Skow, L.C., Hodgkinson, C.A., Arnheiter, H., Copeland, N.G., et al. (1994). Molecular basis of mouse microphthalmia (mi) mutations helps explain their developmental and phenotypic consequences. Nat. Genet. *8*, 256–263.
6. Hughes, A.E., Newton, V.E., Liu, X.Z., and Read, A.P. (1994). A gene for Waardenburg syndrome type 2 maps close to the human homologue of the microphthalmia gene at chromosome 3p12-p14.1. Nat. Genet. *7*, 509–512.
7. Tassabehji, M., Newton, V.E., and Read, A.P. (1994). Waardenburg syndrome type 2 caused by mutations in the human microphthalmia (MITF) gene. Nat. Genet. *8*, 251–255.
8. Tassabehji, M., Newton, V.E., Liu, X.Z., Brady, A., Donnai, D., Krajewska-Walasek, M., Murday, V., Norman, A., Obersztyn, E., Reardon, W., et al. (1995). The mutational spectrum in Waardenburg syndrome. Hum. Mol. Genet. *4*, 2131–2137.
9. Léger, S., Balguerie, X., Goldenberg, A., Drouin-Garraud, V., Cabot, A., Amstutz-Montadert, I., Young, P., Joly, P., Bodereau, V., Holder-Espinasse, M., et al. (2012). Novel and recurrent non-truncating mutations of the MITF basic domain: genotypic and phenotypic variations in Waardenburg and Tietz syndromes. Eur. J. Hum. Genet. *20*, 584–587.
10. Steingrímsson, E., Copeland, N.G., and Jenkins, N.A. (2004). Melanocytes and the microphthalmia transcription factor network. Annu. Rev. Genet. *38*, 365–411.
11. Takebayashi, K., Chida, K., Tsukamoto, I., Morii, E., Munakata, H., Arnheiter, H., Kuroki, T., Kitamura, Y., and Nomura, S. (1996). The recessive phenotype displayed by a dominant negative microphthalmia-associated transcription factor mutant is a result of impaired nucleation potential. Mol. Cell. Biol. *16*, 1203–1211.
12. Grill, C., Bergsteinsdóttir, K., Ogmundsdóttir, M.H., Pogenberg, V., Schepsky, A., Wilmanns, M., Pingault, V., and Steingrímsson, E. (2013). MITF mutations associated with pigment deficiency syndromes and melanoma have different effects on protein function. Hum. Mol. Genet. *22*, 4357–4367.
13. Bharti, K., Gasper, M., Ou, J., Brucato, M., Clore-Gronenborn, K., Pickel, J., and Arnheiter, H. (2012). A regulatory loop involving PAX6, MITF, and WNT signaling controls retinal pigment epithelium development. PLoS Genet. *8*, e1002757.
14. Raviv, S., Bharti, K., Rencus-Lazar, S., Cohen-Tayar, Y., Schyr, R., Evantal, N., Meshorer, E., Zilberberg, A., Idelson, M., Reubinoff, B., et al. (2014). PAX6 regulates melanogenesis in the retinal pigmented epithelium through feed-forward regulatory interactions with MITF. PLoS Genet. *10*, e1004360.
15. Esumi, N., Kachi, S., Campochiaro, P.A., and Zack, D.J. (2007). VMD2 promoter requires two proximal E-box sites for its activity in vivo and is regulated by the MITF-TFE family. J. Biol. Chem. *282*, 1838–1850.
16. Steingrimsson, E., Tessarollo, L., Pathak, B., Hou, L., Arnheiter, H., Copeland, N.G., and Jenkins, N.A. (2002). Mitf and Tfe3, two members of the Mitf-Tfe family of bHLH-Zip transcription factors, have important but functionally redundant roles in osteoclast development. Proc. Natl. Acad. Sci. USA *99*, 4477–4482.
17. Nguyen, M., and Arnheiter, H. (2000). Signaling and transcriptional regulation in early mammalian eye development: a link between FGF and MITF. Development *127*, 3581–3591.
18. Nakayama, A., Nguyen, M.T., Chen, C.C., Opdecamp, K., Hodgkinson, C.A., and Arnheiter, H. (1998). Mutations in microphthalmia, the mouse homolog of the human deafness gene MITF, affect neuroepithelial and neural crest-derived melanocytes differently. Mech. Dev. *70*, 155–166.
19. Izumi, K., Kohta, T., Kimura, Y., Ishida, S., Takahashi, T., Ishiko, A., and Kosaki, K. (2008). Tietz syndrome: unique phenotype specific to mutations of MITF nuclear localization signal. Clin. Genet. *74*, 93–95.
20. Weilbaecher, K.N., Hershey, C.L., Takemoto, C.M., Horstmann, M.A., Hemesath, T.J., Tashjian, A.H., and Fisher, D.E.

(1998). Age-resolving osteopetrosis: a rat model implicating microphthalmia and the related transcription factor TFE3. J. Exp. Med. *187*, 775–785.

21. King, R., Peterson, A.C., Peterson, K.C., Mihm, M.C., Jr., Fisher, D.E., and Googe, P.B. (2002). Microphthalmia transcription factor expression in cutaneous mast cell disease. Am. J. Dermatopathol. *24*, 282–284.
22. Hodgkinson, C.A., Moore, K.J., Nakayama, A., Steingrímsson, E., Copeland, N.G., Jenkins, N.A., and Arnheiter, H. (1993). Mutations at the mouse microphthalmia locus are associated with defects in a gene encoding a novel basic-helix-loop-helix-zipper protein. Cell *74*, 395–404.
23. Niceta, M., Stellacci, E., Gripp, K.W., Zampino, G., Kousi, M., Anselmi, M., Traversa, A., Ciolfi, A., Stabley, D., Bruselles, A., et al. (2015). Mutations Impairing GSK3-Mediated MAF Phosphorylation Cause Cataract, Deafness, Intellectual Disability, Seizures, and a Down Syndrome-like Facies. Am. J. Hum. Genet. *96*, 816–825.

The American Journal of Human Genetics, Volume *99*

Supplemental Data

Biallelic Mutations in *MITF* Cause Coloboma, Osteopetrosis, Microphthalmia, Macrocephaly, Albinism, and Deafness

Aman George, Dina J. Zand, Robert B. Hufnagel, Ruchi Sharma, Yuri V. Sergeev, Janet M. Legare, Gregory M. Rice, Jessica A. Scott Schwoerer, Mariana Rius, Laura Tetri, David M. Gamm, Kapil Bharti, and Brian P. Brooks

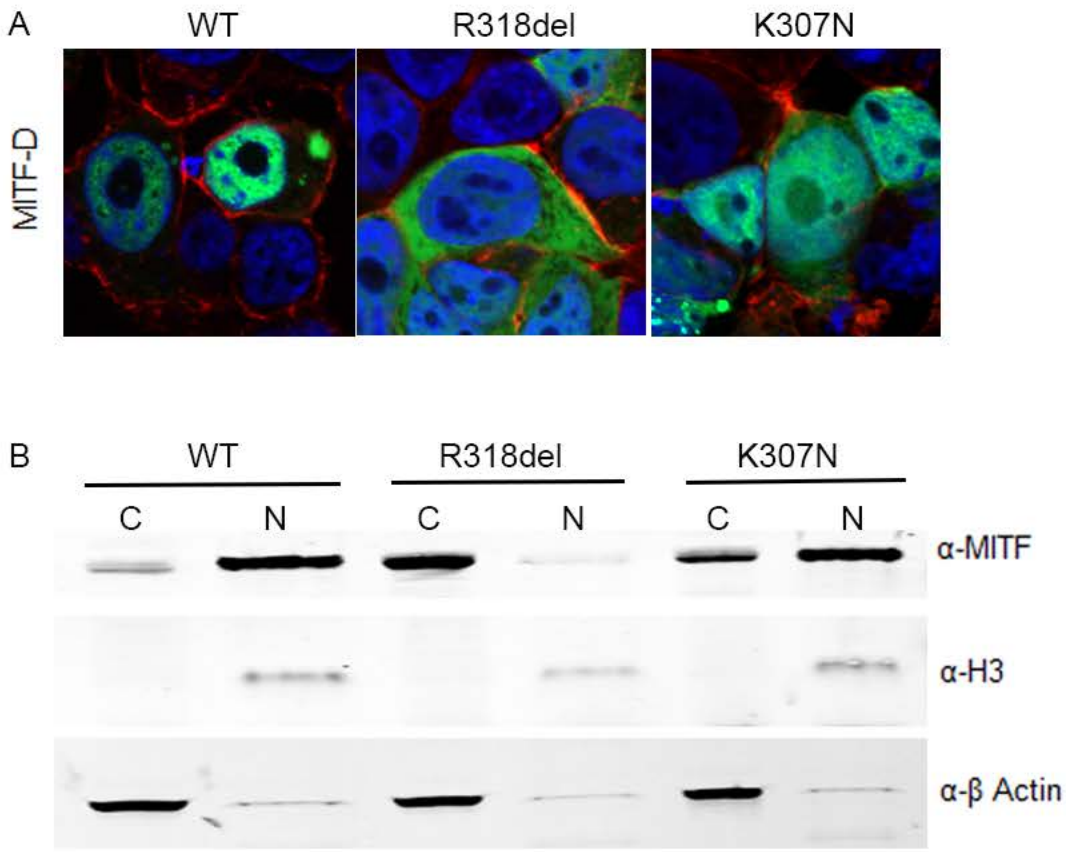
A
WT
R318del
K307N
MITF-D
B
WT
R318del
K307N
C
N
C
N
C
N
α-MITF
α-H3
α-β Actin

Figure S1. Subcellular localization of WT and mutant MITF-D protein.

(A) Green fluorescent protein (GFP) tagged WT-MITF-D isoform was observed predominantly in the nucleus of transfected HEK293 cells. The R318del protein was observed only in the cytoplasm and not in the nucleus, whereas the K307N mutant localized both in the cytoplasm and the nucleus, suggesting some disruption of the nuclear migration ability (also see Supplementary movie). For live cell imaging approximately 1×10^4/well HEK293T cells were cultured in a 4-well glass bottom chamber slide for 24 hrs, and then transiently transfected with fluorescent protein tagged WT and/or mutant MITF constructs. After 24 hrs of transfection, cells were washed three times with cell culture medium and imaged for 15-16 hrs in standard cell culture medium at 37°C and 5% CO2. Every 6 mins, 11 or 13 z-stacks at 20X magnification were acquired in GFP, RFP and DIC channels for each WT and mutant transfection combination using a Zeiss 780 confocal microscope. Time lapse movies were exported from maximum intensity projected Z-image series for each transfection group. The images were analyzed using ZEN Software (Carl Zeiss Microscopy LLC, Thornwood, NY, USA). The experiment was repeated three times for each MITF-A and D. (B) The subcellular localization of mutants was further confirmed by Western blot analysis of the cytoplasmic “C” and nuclear “N” fractions of HEK293 cells transfected by WT and mutant MITF-D isoform, and was observed to be in agreement with the fluorescence microscopy data.

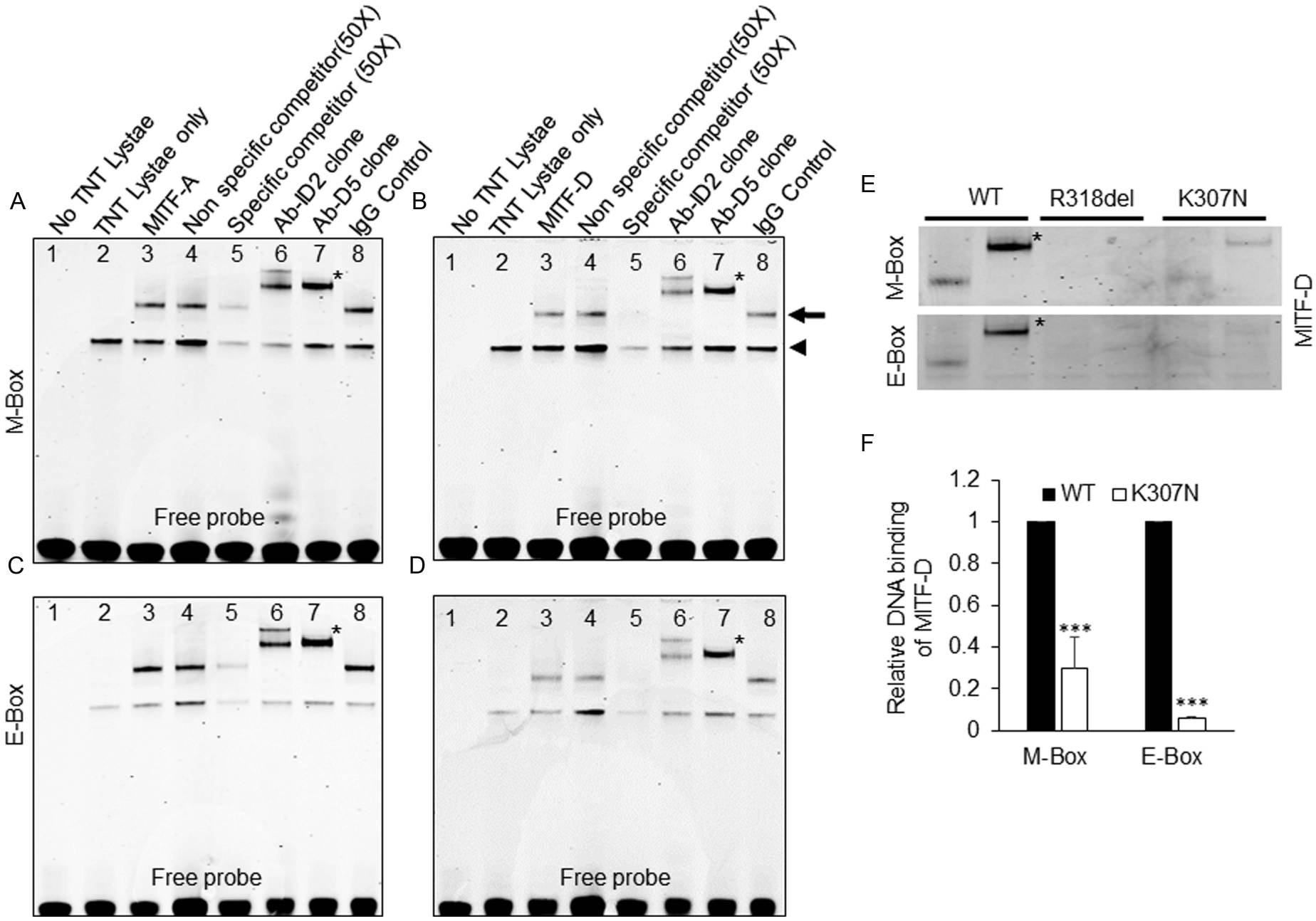
A
No TNT Lystae
TNT Lystae only
MITF-A
Non specific competitor(50X)
Specific competitor (50X)
Ab-ID2 clone
Ab-D5 clone
IgG Control
1 2 3 4 5 6 7 8
M-Box
Free probe
B
No TNT Lystae
TNT Lystae only
MITF-D
Non specific competitor(50X)
Specific competitor (50X)
Ab-ID2 clone
Ab-D5 clone
IgG Control
1 2 3 4 5 6 7 8
Free probe
C
1 2 3 4 5 6 7 8
E-Box
Free probe
D
1 2 3 4 5 6 7 8
Free probe
E
WT
R318del
K307N
M-Box
E-Box
MITF-D
F
Relative DNA binding of MITF-D
WT
K307N
1.2
1
0.8
0.6
0.4
0.2
0
***
***
M-Box
E-Box

Figure S2. Electrophorectic mobility shift assay (EMSA) of WT and mutant MITF (A- and D-isoforms).

(A, B, C and D) EMSAs with *in vitro* translated (IVT) wild type MITF-A and MITF-D proteins incubated with IR-700 labelled probes containing M-Box and E-Box sequences. TnT® reticulocyte lysate alone resulted in a non-specific, shifted band (lane 2, arrowhead) of probe (lane 1), distinct from that observed with IVT MITF protein (lane 3, arrow). Unlabeled nonspecific probe (oligonucleotide with mutated M-Box and E-Box binding site, 50x input, lane 4) did not alter the binding signal, but unlabeled probe (unlabeled oligonucleotide with consensus M-Box and E-Box sequence, 50x input, lane 5), did. Two different anti-MITF antibody clones (ID2 and D5) could supershift (*) the MITF binding signal (lanes 6 & 7, respectively). Supershift was not observed with an IgG control antibody (lane 8). (E and F) The DNA binding ability of MITF-D K307N mutant to the M-Box and E-Box sequence was significantly reduced as compared to the WT-MITF. The R318del mutant did not bind M-Box or E-Box sequences as previously reported. In cases where the DNA binding effect of WT protein + mutant protein was studied, the two proteins were co-transcribed and co-translated, unlike previous report where the proteins are synthesized separately and then mixed later.[1] (F) The graph provides the quantification of the DNA binding by the MITF-D wild type and K307N mutant protein to oligonucleotides carrying consensus M-Box and E-Box elements, as calculated from three different trials. In all comparisons, *P* values were calculated using the Student's *t* test (one sided distribution). ***P<0.005

A

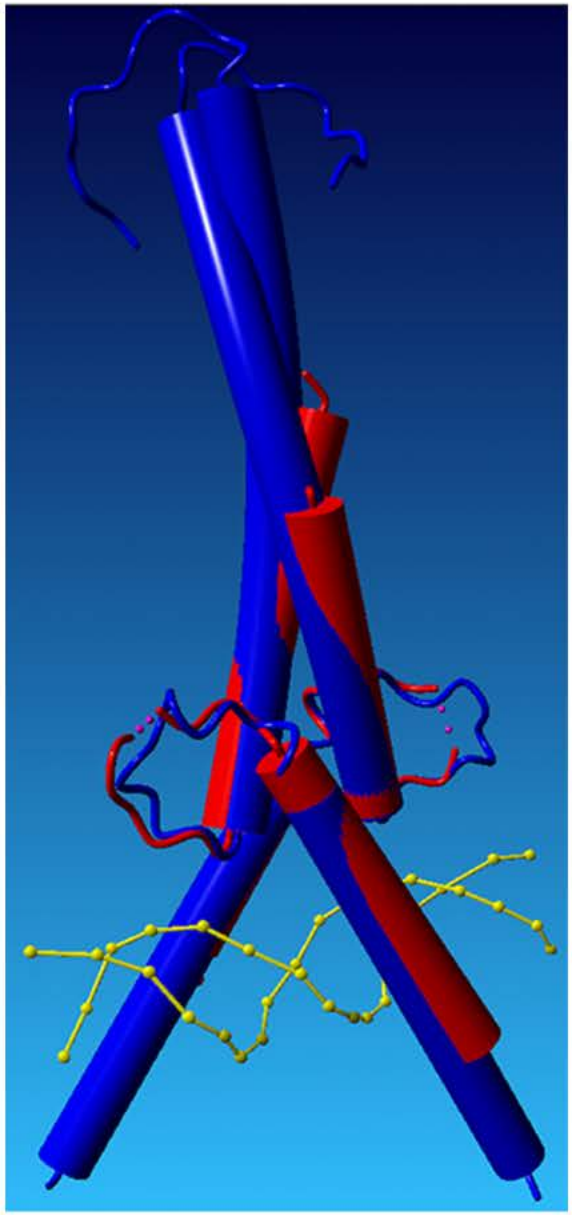

B

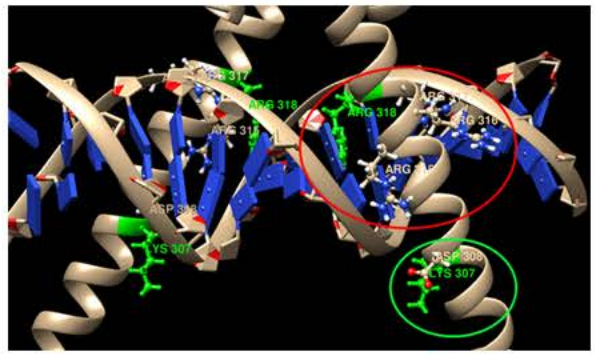
ARG 318
ARG 318
ARG 310
LYS 307
ASP 306
LYS 307

C

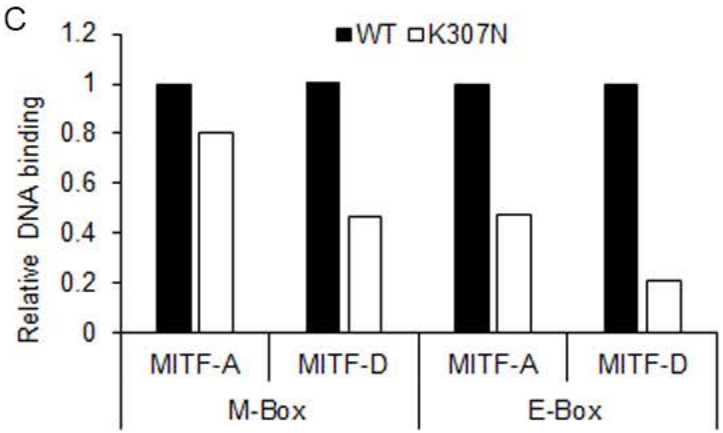
WT
K307N
Relative DNA binding
1.2
1
0.8
0.6
0.4
0.2
0
MITF-A
MITF-D
MITF-A
MITF-D
M-Box
E-Box

D

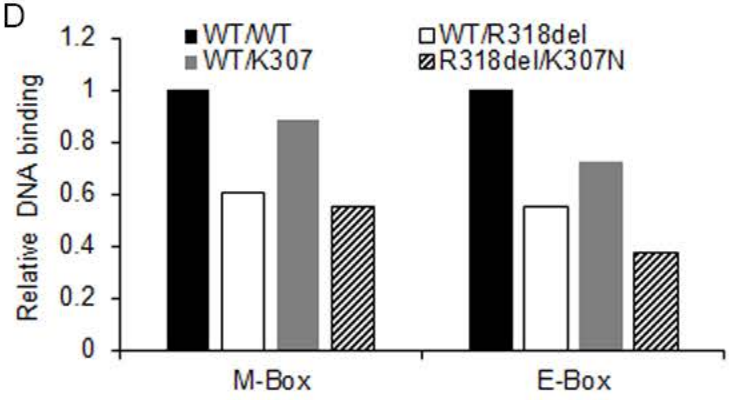
WT/WT
WT/K307
WT/R318del
R318del/K307N
Relative DNA binding
1.2
1
0.8
0.6
0.4
0.2
0
M-Box
E-Box

Figure S3. Molecular modeling of DNA/MITF complexes for four family 1 members

The amino acid sequences of A- and D-isoforms of MITF were retrieved from the UniProtKB database (http://www.uniprot.org/uniprot/O75030). The structures of MITF-DNA homo- and hetero-complexes were generated using molecular visualization, modeling, and dynamics program Yasara[2] (http://www.yasara.org/) and structural templates such as the MITF apo structure (PDB file: 4ATH), MITF: M-box complex (PDB file: 4ATI), and MITF: E-box complex (PDB file: 4ATK). Two wild type complexes and eight mutant variants associated with either the MITF A-isoform or the D-isoform were built as MITF:M-Box or MITF:E-Box homo-dimers. In addition, 16 protein hetero-complexes were built to mimic M-box/E-box complexes formed by the MITF A-isoform: WT/R318del (father), WT/K307N (mother), K307N/R318del (son), WT/WT (daughter); or the MITF D-isoform. All 26 homo- and hetero-complexes were refined, 1 ns equilibrated at 37°C using a 149.4 Å x 89.6 Å x 61.5 Å water box using Amber 99 force field. Finally, binding energy was calculated in aqueous medium as the energy at indefinite distance (between DNA and the rest of the complex) minus the complex energy in the bound state. Molecular visualization was also performed by using the UCSF Chimera (http://www.cgl.ucsf.edu/chimera/). (A) The structure of wild type MITF-A isoform bound to the consensus E-box DNA sequence was prepared by molecular modeling (represented in blue) using the already available crystallographic structure of MITF-M as a template (shown in red). The two structures were then merged to represent the fitness of the modelling. Other complexes comprising of mutant MITF-A isoforms, and wild type and mutant MITF-D isoforms bound to the DNA were built (data not shown), as described in methods section. (B) The Needleman-Wunsch structural alignment shows a loose structural fitting of the deletion mutant to the crystallographic template (root mean square of 3.2 Å), compared to that of a wild type or the variant with missense mutation

in both MITF-A and –D isoforms (r.m.s. of 0.9-1.5 Å). This observation suggests that deletion in position 318 causes a more significant change in the subunit structure than that of the K307N mutant. (C) Initial comparison of WT and mutant MITF protein models predicts a trend of decreasing DNA binding of homodimers to the DNA in the following order: wt/wt>K307N/K307N>R318del/R318del. Moreover the 15 ns equilibration of the deletion mutant complex shows complex dissociation and complete loss of DNA binding (data not shown). This suggests that deletion variants do not favor a DNA binding complex and agree with the observation that R318del variant does not bind DNA (therefore not shown in the graph C). (D) In case of the WT/mutant combination, three different complexes i.e. WT+WT, WT+mutant and mutant+mutant, are possible. The binding energy, for each of these complexes was determined using molecular modelling since it could not have been done experimentally. The observed binding energies were then combined for all of the patient genotypes and were consistent with the EMSA data (Figure 3C graph).

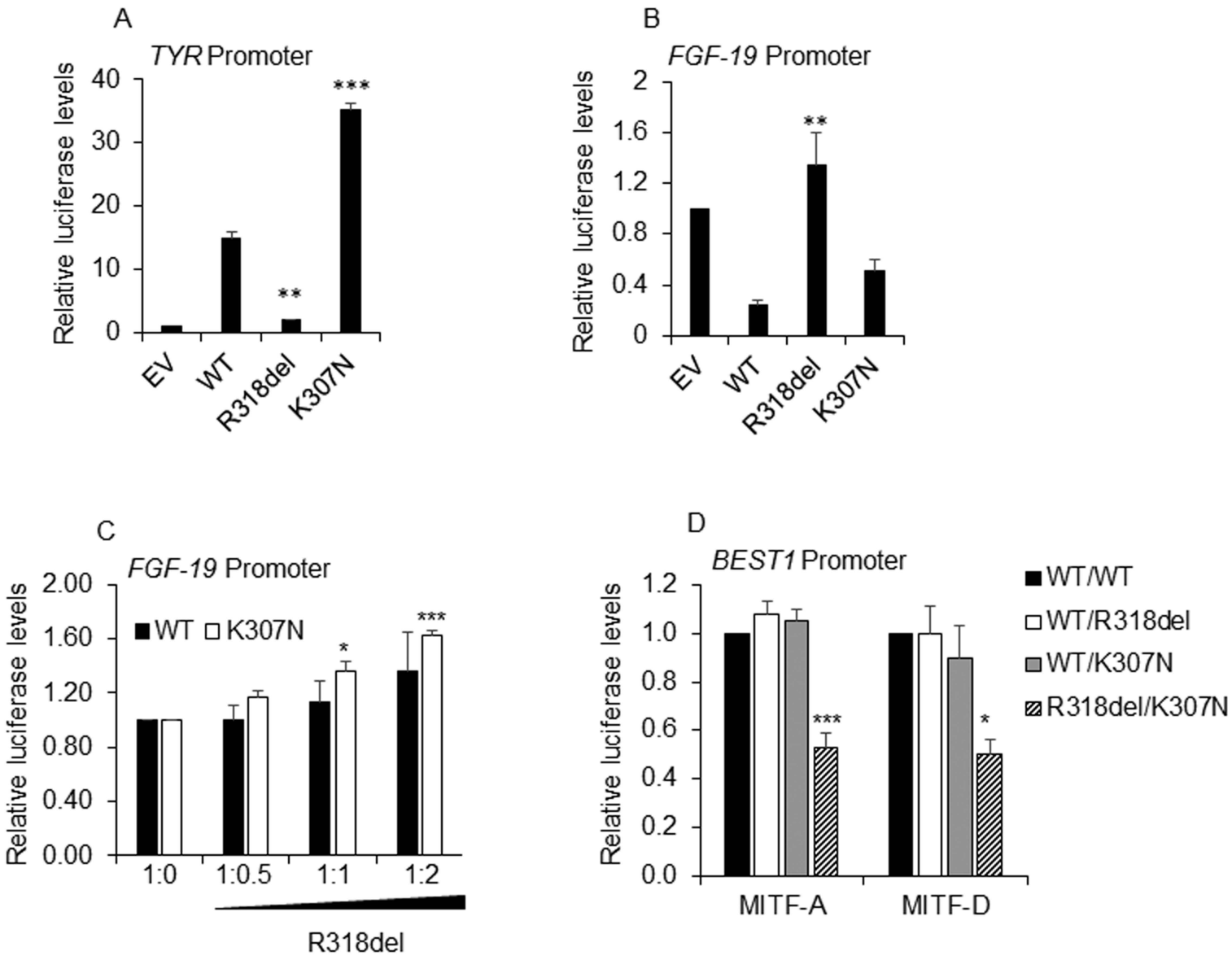
A
TYR Promoter
Relative luciferase levels
40
30
20
10
0
***
**
EV
WT
R318del
K307N
B
FGF-19 Promoter
Relative luciferase levels
2
1.6
1.2
0.8
0.4
0
**
EV
WT
R318del
K307N
C
FGF-19 Promoter
Relative luciferase levels
2.00
1.60
1.20
0.80
0.40
0.00
WT
K307N
*
***
1:0
1:0.5
1:1
1:2
R318del
D
BEST1 Promoter
Relative luciferase levels
1.2
1.0
0.8
0.6
0.4
0.2
0.0
***
*
MITF-A
MITF-D
WT/WT
WT/R318del
WT/K307N
R318del/K307N

Figure S4. Transactivation of MITF-responsive genes by WT and mutant MITF protein.

(A and B) The K307N mutant protein activated the *TYROSINASE* (*TYR)* promoter more than WT MITF and repressed the *FGF-19* promoter. The R318del mutant or empty vector (EV) did not activate nor repressed the studied promoters. (C) Repression of *FGF-19* gene promoter by WT and K307N mutant MITF-A in the presence of R318del mutant. The R318del mutant in increasing concentrations (0, 50, 100 and 200 ng) caused de-repression of FGF-19 promoter by WT-MITF (solid bars, statistically not significant). This is evident by the increase in *FGF-19* promoter trans-activation with increasing concentration of R318del mutant. In contrast, a similar de-repression caused by increasing concentrations of R318del in the presence of K307N was observed to be statistically significant (open bars, $P<0.005$). (D) Transactivation of the RPE specific *Best1* promoter by combination of WT and mutant MITF. Mouse MITF is known to activate the murine *Best1* gene promoter, specific to the retinal pigmented epithelium. A dual luciferase assay was performed to study the effect of the MITF mutation combinations (similar to the genotype of members of family 1) on the activation of this promoter. HEK293 cells were co-transfected with equal amounts of WT and mutant MITF isoforms or the two mutants together with the *Best1* luciferase promoter construct. The promoter activation was observed to be significantly reduced when the two mutants (corresponding to the genotype of proband I) were transfected. Interestingly the relative luciferase levels were similar for the WT/mutant (genotype of affected parents) combinations and WT alone (genotype of unaffected sibling). All comparisons are in reference to the WT-MITF, *P* values were calculated using the two-sided Student's *t* test. *$P<0.05$, **$P<0.01$, ***$P<0.005$.

Table S1: Sequences of the primers and probes used in the study.

Primers/ probes	**Sequence**	
MITF-A	5'-GCGGGAAAGCTTCAGTCCGAATCGGGGATCG-3'	Forward
MITF-D	5'-CCTCCAAGCTTACATCACGCATCTTGCTACG-3'	Forward
MITF-A & D	5'-GGGAGTCTAGACTAACAAGTGTGCTCCGTCTC-3'	Reverse
MITF-A	5'ATGGACTACAAAGACGATGACGACAAGGCGGGAAAG CTTCAGTCCGAATCGGGGATCG-3'	Forward
MITF-D	5'ATGGACTACAAAGACGATGACGACAAGCCTCCAAGCT TACATCACGCATCTTGCTACG -3'	Forward
MITF-A & D	5'-ATAGACCCGGGAGTGTGCTCCGTC-3'	Reverse
M-Box	5'-IR700/GAAAAGTCAGTCATGTGCTTTTCAG-3'	Probe
E-Box	5'- IR700/AAAGAGTAGCACGTGCTACTCAGA-3'	Probe

References

1. Vachtenheim, J. and Drdová, B. *Pigment Cell Res.* **17**, 43-50 (2004).

2. Krieger, E. *et al. Proteins* **47**, 393–402 (2002).